RESEARCH ARTICLE

Actinomycin D Targets NPM1c-Primed Mitochondria to Restore PML-Driven Senescence in AML Therapy

Hsin-Chieh Wu[1,2], Domitille Rérolle[1,2], Caroline Berthier[1,2], Rita Hleihel[1,2,3,4], Takashi Sakamoto[5,6], Samuel Quentin[2], Shirine Benhenda[2], Claudia Morganti[7], Chengchen Wu[1,2], Lidio Conte[1,2,8], Sylvie Rimsky[1], Marie Sebert[2,9], Emmanuelle Clappier[2,9], Sylvie Souquere[10], Stéphanie Gachet[2], Jean Soulier[2,9], Sylvère Durand[10], Jennifer J. Trowbridge[11], Paule Bénit[12], Pierre Rustin[12], Hiba El Hajj[4], Emmanuel Raffoux[9], Lionel Ades[2,9], Raphael Itzykson[2,9], Hervé Dombret[9], Pierre Fenaux[2,9], Olivier Espeli[1], Guido Kroemer[8,13,14], Lorenzo Brunetti[15], Tak W. Mak[6], Valérie Lallemand-Breitenbach[1,2], Ali Bazarbachi[3], Brunangelo Falini[15], Keisuke Ito[7], Maria Paola Martelli[15], and Hugues de Thé[1,2,9]

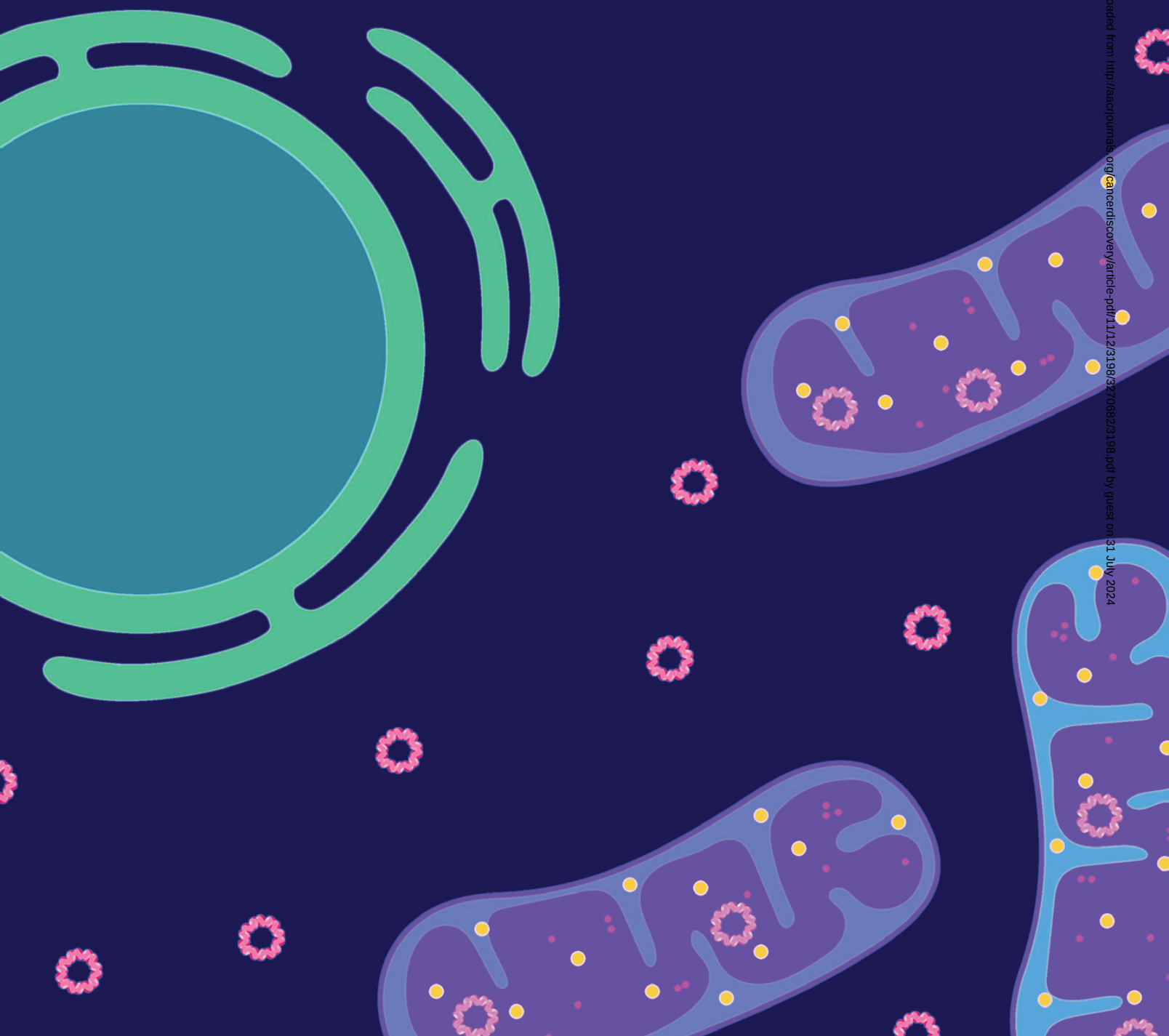

ABSTRACT Acute myeloid leukemia (AML) pathogenesis often involves a mutation in the NPM1 nucleolar chaperone, but the bases for its transforming properties and overall association with favorable therapeutic responses remain incompletely understood. Here we demonstrate that an oncogenic mutant form of NPM1 (NPM1c) impairs mitochondrial function. NPM1c also hampers formation of promyelocytic leukemia (PML) nuclear bodies (NB), which are regulators of mitochondrial fitness and key senescence effectors. Actinomycin D (ActD), an antibiotic with unambiguous clinical efficacy in relapsed/refractory NPM1c-AMLs, targets these primed mitochondria, releasing mitochondrial DNA, activating cyclic GMP-AMP synthase signaling, and boosting reactive oxygen species (ROS) production. The latter restore PML NB formation to drive TP53 activation and senescence of NPM1c-AML cells. In several models, dual targeting of mitochondria by venetoclax and ActD synergized to clear AML and prolong survival through targeting of PML. Our studies reveal an unexpected role for mitochondria downstream of NPM1c and implicate a mitochondrial/ROS/PML/TP53 senescence pathway as an effector of ActD-based therapies.

SIGNIFICANCE: ActD induces complete remissions in NPM1-mutant AMLs. We found that NPM1c affects mitochondrial biogenesis and PML NBs. ActD targets mitochondria, yielding ROS which enforce PML NB biogenesis and restore senescence. Dual targeting of mitochondria with ActD and venetoclax sharply potentiates their anti-AML activities *in vivo*.

INTRODUCTION

The nucleolar chaperone nucleophosmin 1 (NPM1) exerts a wide range of activities, from ribosome biogenesis to control of MYC or TP53 signaling. In 50% of acute myeloid leukemia (AML) with normal karyotypes, highly clustered monoallelic *NPM1* mutations cause frameshifts that delete tryptophan residues involved in nucleolar targeting and create *de novo* nuclear export signals (1). While occurrence of cytoplasmic NPM1 (NPM1c) oncoprotein is preceded by mutations sustaining clonal hematopoiesis (2), its continuous presence is required for maintaining the leukemic state of established AMLs, where NPM1c disables TP53 signaling and sustains high expression of HOX genes (3).

Promyelocytic leukemia (PML) nuclear bodies (NB) are reactive oxygen species (ROS)–responsive domains (4, 5) that exert prosenescent and tumor-suppressive functions by enhancing TP53 and Rb activities. Many protein degradation pathways associated with tumor progression target PML, presumably to impede its prosenescent function. PML NBs have directly been implicated in the therapeutic response of acute promyelocytic leukemia (APL) where the PML/RARA fusion oncoprotein disrupts PML bodies, but therapy-induced PML/RARA degradation restores them to drive cure (6–8). PML has also been implicated in tumor robustness through the control of mitochondrial fitness and stem cell metabolism (9–11).

Mitochondrial dysfunctions can induce the integrated stress response and ROS production, important features of normal or AML stem cells (12). Conversely, mitochondrial fitness and high oxidative phosphorylation (OXPHOS) metabolism have been implicated in resistance to BCL2 inhibitors or conventional chemotherapy (13–18). Accordingly, inhibitors of mitochondrial respiration were proposed to constitute a novel type of cancer drugs (19). In addition to their well-studied effects on nuclear DNA replication or transcription, anticancer antibiotics may exert ill-understood mitochondrial toxicities, implicated in long-term doxorubicin-induced cardiomyocyte loss (20).

Here, we demonstrate that NPM1c blunts PML NB biogenesis and weakens mitochondrial fitness. Actinomycin D (ActD), a drug with established clinical activity in

[1]Collège de France, Oncologie Cellulaire et Moléculaire, PSL University, INSERM UMR 1050, CNRS UMR 7241, Paris, France. [2]Université de Paris, INSERM U944, CNRS UMR 7212, IRSL, Hôpital St. Louis, Paris, France. [3]Department of Internal Medicine and Department of Anatomy, Cell Biology and Physiological Sciences, American University of Beirut, Beirut, Lebanon. [4]Department of Experimental Pathology, Microbiology and Immunology, American University of Beirut, Beirut, Lebanon. [5]Department of Hematology and Oncology, Graduate School of Medicine, Kyoto University, Kyoto, Japan. [6]Princess Margaret Cancer Centre, University Health Network, Toronto, Ontario, Canada. [7]Ruth L. and David S. Gottesman Institute for Stem Cell and Regenerative Medicine Research and Departments of Cell Biology and Medicine, Albert Einstein College of Medicine, Bronx, New York. [8]Department of Precision Medicine, University of Campania "Luigi Vanvitelli," Napoli, Italy. [9]Department of Hematology, Hôpital Saint Louis (Assistance publique Hôpitaux de Paris) and Paris University, Paris, France. [10]Institut Gustave Roussy, Cell Biology and Metabolomics Platforms, INSERM UMS 3655, Villejuif, France. [11]The Jackson Laboratory, Bar Harbor, Maine. [12]INSERM, U1141 Hôpital Robert Debré, Paris France. [13]Centre de Recherche des Cordeliers, Equipe labellisée par la Ligue Contre le Cancer, Université de Paris, Sorbonne Université, INSERM U1138, Institut Universitaire de France, Paris, France. [14]Pôle de Biologie, Hôpital Européen Georges Pompidou, AP-HP, Paris, France. [15]Hematology, Department of Medicine and surgery, University of Perugia, Perugia, Italy.

D. Rérolle, C. Berthier, R. Hleihel, and T. Sakamoto contributed equally as co-second authors of this article.

Corresponding Author: Hugues de Thé, Collège de France, 11 Place Marcellin Berthelot, Paris 75005, France. Phone: 33-680667389; E-mail: hugues.dethe@inserm.fr

Cancer Discov 2021;11:3198–213

doi: 10.1158/2159-8290.CD-21-0177

therapy-resistant NPM1c-AML (21–23), induces acute mitochondrial stress, ROS production, restoration of PML NBs, and senescence, contributing to its therapeutic efficacy.

RESULTS

NPM1c Targets PML and Promotes Cell Growth

Primary leukemic cells or cell lines from patients with AML expressing NPM1c exhibit some defects in NB formation, resembling APL micro-speckles (refs. 24, 25; Supplementary Fig. S1A and S1B). As AMLs harbor multiple gene mutations that may contribute to NB alteration, we explored nonleukemic primary hematopoietic stem cells (HSC) from a Flp-inducible humanized Npm1c (variant A) knock-in mouse model (*Npm1*$^{frt\text{-}cA/+}$, *R26*^{FlpoER}; ref. 26). Four weeks after tamoxifen exposure, these HSCs exhibited a dramatic reduction of NB numbers (Fig. 1A). Similarly, hematopoietic progenitors that were differentiated from a mouse embryonic stem cell (mESC) NPM1c knock-in model (Supplementary Fig. S1C) displayed significantly fewer PML NBs.

A previous study suggested that overexpressed PML and NPM1c may interact (27). Transient expression of NPM1c (but not NPM1) disrupted PML NBs in mouse embryonic fibroblasts (MEF) stably expressing GFP-PML-III (Fig. 1B). Cysteine 288 in the *de novo* C-terminal sequence of NPM1c was implicated in nucleolar export and oxidative stress control (28). Mutation of this residue in NPM1c abolished its ability to oppose NB formation (Fig. 1B). Conversely, an exquisitely redox-sensitive cysteine residue of PML (C389; ref. 29) was required for NPM1c to target NBs. Immunoprecipitation experiments demonstrated that ectopically expressed NPM1c interacts with PML, a process that requires NPM1c C288 and PML C389, but not a PML cysteine residue implicated in arsenic binding (ref. 4; Fig. 1C and D). We determined whether a disulfide bond might govern interaction of NPM1c with PML. For this, we transiently transfected PML and NPM1 variants and purified His-PML proteins under denaturing conditions, followed by NPM1 Western blot analyses, in the absence or presence of the protein-reducing agent TCEP. High molecular weight complexes reactive with both PML and NPM1c antibodies were detected only when NPM1c C288 and PML C389 were both present and TCEP was omitted (Fig. 1E; Supplementary Fig. S1D). Thus, two reactive cysteines in NPM1c and PML interact, yielding impairment of PML NB assembly. However, while NPM1c binding is required for PML NB disruption, cytoplasmic localization of NPM1c did not require PML, as observed in *NPM1c* knock-in *Pml*$^{-/-}$ mESCs (Supplementary Fig. S1E).

To explore functional consequences of NPM1c–PML interactions, we generated an isogenic system by stably expressing GFP-NPM1c, GFP-NPM1c^{C288S}, or GFP-NPM1 fusions in OCI-AML2 leukemic cells (hereafter named AML2) in which *NPM1* gene is wild-type (WT). Expression of NPM1c blunted NB formation, whereas NPM1c^{C288S} failed to do so (Fig. 1F). Functionally, expression of NPM1c, but not NPM1c^{C288S}, increased clonogenic activity in methylcellulose cultures (Fig. 1G) and activated E2F and MYC target genes (Fig. 1H; Supplementary Table S1), possibly reflecting decreased basal level of TP53 and ARF (Fig. 1I). NPM1c expression also diminished PML protein levels (but not *PML* mRNA; Supplementary Fig. S1F). Low PML protein expression was confirmed in primary AML patient samples (Fig. 1J) and could independently amplify NPM1c-driven defects of PML NB formation. Finally, NPM1c reduced expression of WT NPM1 (Fig. 1I), which, in NPM1c AML blasts, may further aggravate *NPM1* haploinsufficiency (30).

NPM1c Affects Mitochondria and Drives Stress Response

Because NPM1c impairs NB biogenesis and PML NBs control mitochondrial fitness (9, 10), we assessed the impact of NPM1c expression on mitochondrial status. In tamoxifen-treated NPM1c knock-in mice (26), we found an increase in mitochondrion number (but not volume) in phenotypic HSCs, but not in Lin-negative cells (Fig. 2A; Supplementary Fig. S2A). Similarly, in NPM1c-expressing isogenic AML2 cells, the number of mitochondria increased, while the branching pattern decreased (Fig. 2B) and cristae were lost, as determined by transmission electron microscopy (Fig. 2C). Transcriptomic and proteomic analyses revealed dysregulation of mitochondria-related pathways (Supplementary Fig. S2B). These mitochondrial defects were associated with enhanced production of ROS, mitochondrial superoxides, and membrane potential, with no alteration of mitochondrial mass (Fig. 2D; Supplementary Fig. S2C). Mitochondrial impairment was also substantiated by leakage of mitochondrial DNA (mtDNA) into the cytoplasm in NPM1c-expressing AML2 or mESCs (Fig. 2E; Supplementary Fig. S2D) and reduced electron transport chain (ETC) proteins, notably complex II, reflecting transcriptional downregulation of *SDH* genes (Supplementary Fig. S2E–S2G).

Release of mtDNA into the cytoplasm was associated with the ignition of intracellular stress pathways, particularly cyclic GMP-AMP (cGAMP) synthase (cGAS) activation, and cGAMP production, resulting in the downstream transcriptional activation of IFN and NFκB pathways (Fig. 2F–H; refs. 31, 32). Other stress pathways, such as oxidative stress and unfolded protein response (UPR), were also activated (Fig. 2H; Supplementary Fig. S2B; Supplementary Tables S2 and S3), explaining the decrease in global protein synthesis (Fig. 2I). Western blot analyses validated activation of these stress pathways in AML2-NPM1c cells, including the upregulation of key TP53-repressed metabolic enzymes (Supplementary Fig. S2H). As expected, these mitochondrial alterations decreased the ATP/ADP ratio, reflecting metabolic stress (Fig. 2J). Functionally, activation of these stress pathways could favor AML cell fitness (12). Indeed, inhibition of cGAS activity by G140 selectively suppressed growth of AML2-NPM1c cells (Supplementary Fig. S2I).

Mechanistically, two key regulators of mitochondrial protein expression, PPARγcoactivator 1-alpha (*PGC1A*) and transcription factor A mitochondrial (*TFAM*), showed decreased protein abundance in AML2-NPM1c (Fig. 2K) and OCI-AML3 cells (hereafter referred as AML3, which are NPM1c mutant) when compared with AML2 cells (Supplementary Fig. S2J). TFAM reduction may reflect transcriptional downregulation of *PGC1A* by IFN signaling (33). Importantly, stable NPM1c expression in AML2 cells drove PGC1α hyperacetylation resulting in its functional inactivation, a known consequence of PML NB downregulation (Fig. 2L; refs. 9, 10).

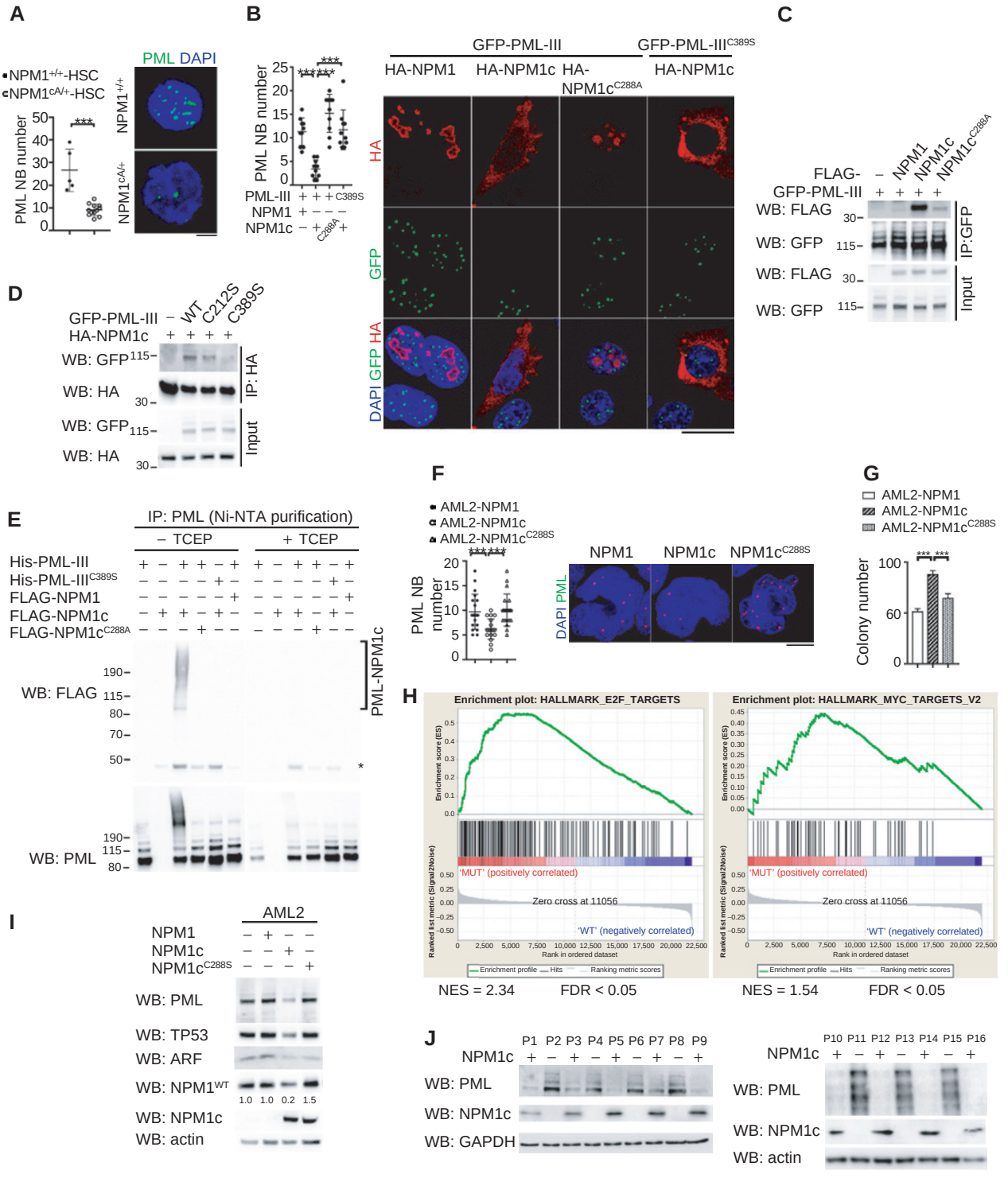

Figure 1. NPM1c alters PML NBs biogenesis. **A,** Quantification (left) and representative image (right) of PML NBs in HSCs purified from NPM1c-expressing knock-in mice. The results are expressed as the mean value ± SD (error bars) of $n = 5$ $NPM1^{+/+}$ and 12 $NPM1^{cA/+}$ mice. Unpaired *t* test; ***, $P < 0.001$. Scale bar, 3 μm. **B,** Quantification (left) and representative image (right) of PML NBs in MEFs stably expressing GFP-PML-III and transiently transfected with NPM1-derived expression vectors. Results are expressed as the mean value ± SD (error bars) of $n = 8$ analyzed cells per condition. Unpaired *t* test; ***, $P < 0.001$. Scale bar, 10 μm. **C** and **D,** Coimmunoprecipitation analyses of 293T cells transfected with indicated constructs. **E,** Histidine pulldown of disulfide-linked NPM1c–PML complex from transiently transfected 293T cells. *, nonspecific binding to NPM1. **F,** Quantification (left) and representative image (right) of PML NBs in isogenic AML2 derivatives. Results are expressed as the mean value ± SD (error bars) of $n = 18$ analyzed cells per condition. Unpaired *t* test; ***, $P < 0.001$. Scale bar, 10 μm. **G,** Colony-forming ability of isogenic AML2 derivatives. Unpaired *t* test. $n = 3$. **H,** GSEA analyses of E2F and MYC pathways in transcriptomic exploration of NPM1c versus NPM1-expressing AML2 cells. **I,** Western blot analyses of TP53, ARF, PML, and endogenous NPM1 in isogenic AML2 cells. Quantification of WT NPM1 is shown. **J,** Western blot analyses of PML in primary bone marrow samples from 9 NPM1c and 7 NPM1 AML samples explored.

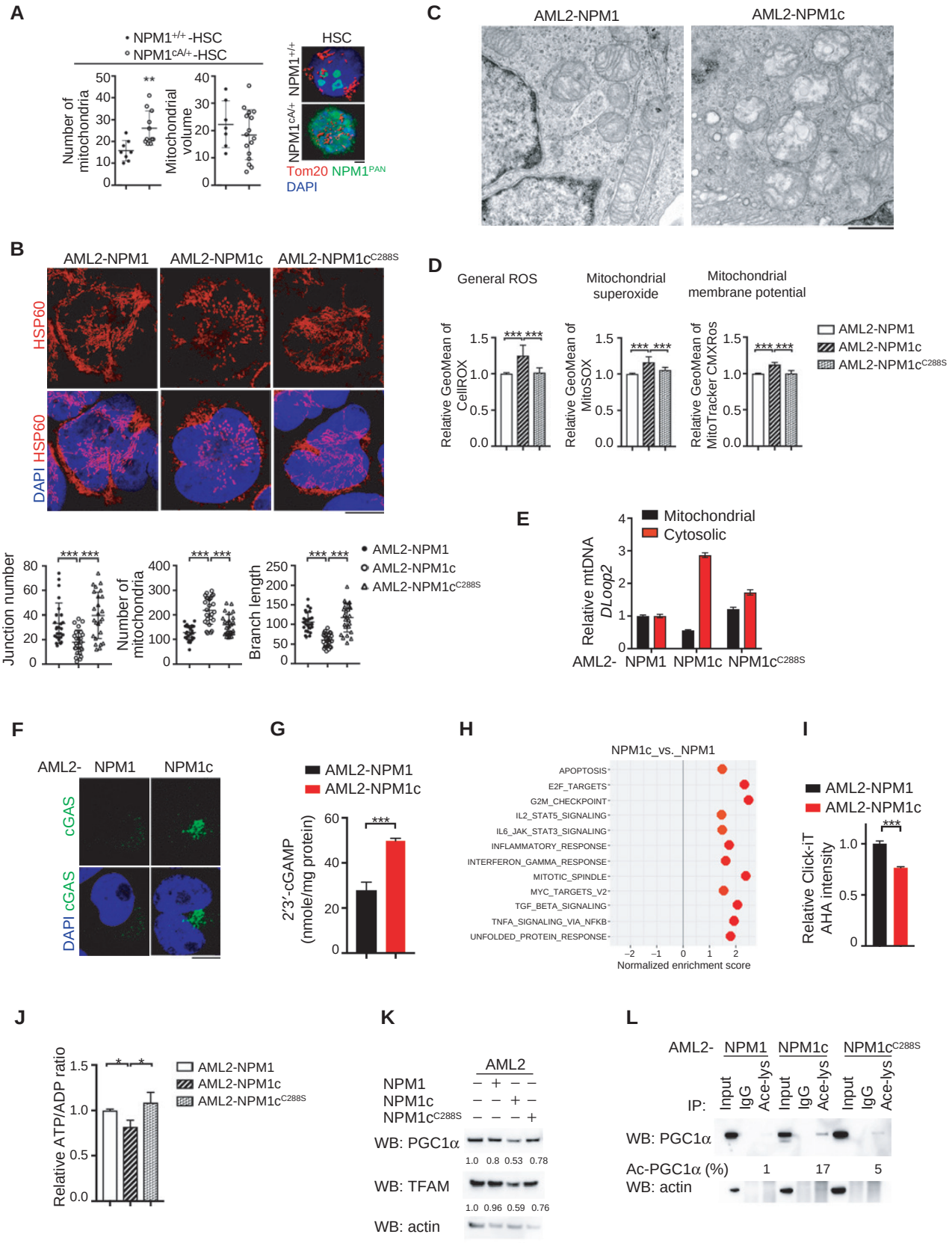

In principle, NPM1c could alter mitochondrial functions independently from its ability to interfere with PML NB formation. Exploring mitochondrial status in *NPM1c*-knockins *Pml*$^{+/+}$ or *Pml*$^{-/-}$ mESCs revealed that mitochondrial morphology was so profoundly altered in *Pml*$^{-/-}$ mESCs that it precluded further detection of NPM1c-driven abnormalities (Supplementary Fig. S2K).

ActD Targets Mitochondria and Promotes Superoxide Response

Recent clinical studies have shown that the rDNA transcriptional inhibitor ActD can induce complete remissions and even cure some patients with refractory/relapsed NPM1c-AML as a single agent (21–23). Transcriptional inhibition of rDNA genes by ActD induces nucleolar segregation and activates TP53 through ribosomal checkpoint activation upon MDM2–L5/L11 complex formation (34). When used at low doses (1–10 nmol/L), ActD triggers a transient cell-cycle arrest in the absence of TP53 stabilization, DNA damage, or apoptosis (35). We found that 5 nmol/L ActD (a concentration in the range of those found in patients; ref. 23) triggered TP53 activation in AML3, but not in AML2 cells (Supplementary Fig. S3A). Nonetheless, we observed only a small increase in the L11–HDM2 interaction in patient *in vivo* (see below), suggesting that ribosomal checkpoint activation may not solely account for TP53 activation (Supplementary Fig. S3B). Unexpectedly, we found that ActD treatment rapidly fragmented the mitochondrial network in AML3 or NPM1c-mESCs, with no or minor effects in AML2 or mESCs (Fig. 3A; Supplementary Fig. S3C and S3D). Moreover, ActD initiated rapid production of ROS and induction of a superoxide transcriptional response, loss of mitochondrial membrane potential, and loss of mtDNA through its leakage to the cytoplasm, all preferentially in AML3 and/or AML2-NPM1c cells (Fig. 3B–F), with little immediate effect on mitochondrial DNA expression (Supplementary Fig. S3E).

ActD-triggered mitochondrial toxicity drove stress responses, as indicated by increased cGAMP production, phosphorylation of eIF2α (Fig. 3G and H), transcriptional stress signatures (UPR, ROS signaling), activation of innate immunity (IFN, TNFA, and TGFB; ref. 36), and apoptosis/senescence (TP53; Supplementary Fig. S3F). While responses were often shared between the two isogenic cell lines, IFN and TP53 activation were particularly pronounced in AML2-NPM1c cells. We found a remarkable similarity between the basal expression of genes induced by NPM1c and those activated by ActD in AML2 cells (Supplementary Fig. S3G), likely reflecting their shared ability to impair mitochondrial function. Consequently, ActD-triggered induction of stress pathways may be functionally more significant in NPM1c-expressing cells where basal activation levels are already high. Finally, ActD exacerbated preexisting NPM1c-driven metabolic stress, as revealed by decreased ATP levels and increased AMP-activated protein kinase (AMPK) phosphorylation (Fig. 3I and J). Collectively, these observations suggest that ActD targets mitochondria, particularly those primed by NPM1c expression.

ActD Activates a ROS/PML/TP53 Senescence Axis in NPM1c-Expressing Cells *Ex Vivo*

We then explored the cellular impacts of mitochondrial poisoning by ActD. Unexpectedly, ActD rapidly restored PML NBs in NPM1c-transfected MEFs, AML2-NPM1c or AML3 cells (Fig. 4A; Supplementary Fig. S4A). PML NB restoration was also observed in primary NPM1c-AML blasts treated *ex vivo* with ActD (Fig. 4B). In transiently transfected cells, NB restoration by ActD was associated with (and likely caused by) disruption of NPM1c-PML complexes (Fig. 4C). Similarly, in AML3 cells, ActD (as TCEP) restored the normal size of high molecular weight NPM1 or PML species (Supplementary Fig. S4B). Apart from disrupting NPM1c–PML adducts, ActD-induced ROS may also directly enforce PML NB biogenesis (4, 5). Accordingly, NB restoration in AML2-NPM1c cells was blocked by the ROS scavengers N-acetyl cysteine (NAC) and glutathione (Supplementary Fig. S4C).

PML NBs are tightly linked to senescence induction. In AML3 cells, ActD-driven PML NB reformation was associated to multiple signs of senescence, including TP53 activation, increase in p21 or *Serpine-1* expression, activation of senescence-associated β-galactosidase (SA-β-Gal) activity, and loss of clonogenic potential (Fig. 4D–F; Supplementary Fig. S4D). Importantly, these features were abolished or attenuated by *PML* or *TP53* deletion. Moreover, blocking PML NB reformation with antioxidants blunted ActD-driven TP53 and P21 activation, as well as loss of clonogenic activity (Fig. 4G and H). Collectively, these experiments establish a central role of a ROS/PML/TP53 cascade in driving senescence and ActD response *ex vivo*.

To substantiate the mitochondrial origin of ActD-induced ROS in driving TP53 activation, we cultured AML cells with low-dose antimycin A (Fig. 4I) to promote progressive

Figure 2. NPM1c affects mitochondria and drives an integrated stress response. **A,** Number and volume of mitochondria in HSCs purified from NPM1c-knockin mice. The results are expressed as the mean value ± SD (error bars) of $n = 8$ NPM1$^{+/+}$ and 11 NPM1$^{cA/+}$ HSC. Unpaired *t* test; **, $P < 0.005$. Scale bar, 3 μm. **B,** Examination of mitochondrial morphology in NPM1-, NPM1c-, and NPM1c^{C288S}-expressing AML2 cells. Top, immunofluorescence analyses of mitochondrial morphology. Bottom, mitochondrial fragmentation was quantified by number of mitochondria, of junctions and branch length. The results are expressed as the mean value ± SD (error bars) of $n = 25$ cells per condition. Unpaired *t* test; ***, $P < 0.001$. Scale bar, 10 μm. **C,** Transmission electron microscopy image of mitochondrial cristae in AML2-derived isogenic cells. Scale bar, 1 μm. **D,** FACS analyses of mitochondrial status in AML2-derived isogenic lines. The results from are expressed as the mean value ± SD of three independent experiments. Unpaired *t* test; ***, $P < 0.001$; **, $P < 0.01$. **E,** Quantification of cytosolic and mitochondrial mtDNA. The results are expressed as the mean value of triplicate samples ± SD. Unpaired *t* test; ***, $P < 0.001$; $n = 3$. **F,** Immunofluorescence analyses of cGAS localization in NPM1c cells. **G,** Basal 2′3-cGAMP concentration in AML2 cells expressing NPM1c or not. The results are expressed as the mean value of triplicate samples ± SD. Unpaired *t* test. ***, $P < 0.001$. $n = 2$. **H,** GSEA of differentially expressed genes in AML2 cells expressing NPM1c or not. **I,** Effect of NPM1c expression on nascent protein synthesis. The results are expressed as the mean value of triplicate samples ± SD. Unpaired *t* test; ***, $P < 0.001$; $n = 3$. **J,** ATP/ADP ratio in AML2-derived isogenic lines. The results are expressed as the mean value of triplicate samples ± SD. Unpaired *t* test; *, $P < 0.05$. **K,** Western blot analyses of TFAM and PGC1α in AML2-derived isogenic cells. Quantification of acetylated PGC1a is shown. **L,** Acetylation of PGC1α in isogenic AML2 cells. Immunoprecipitation of lysine-acetylated proteins followed by Western blot with an anti-PGC1α antibody. The estimated fraction of acetylated PGC1α is indicated.

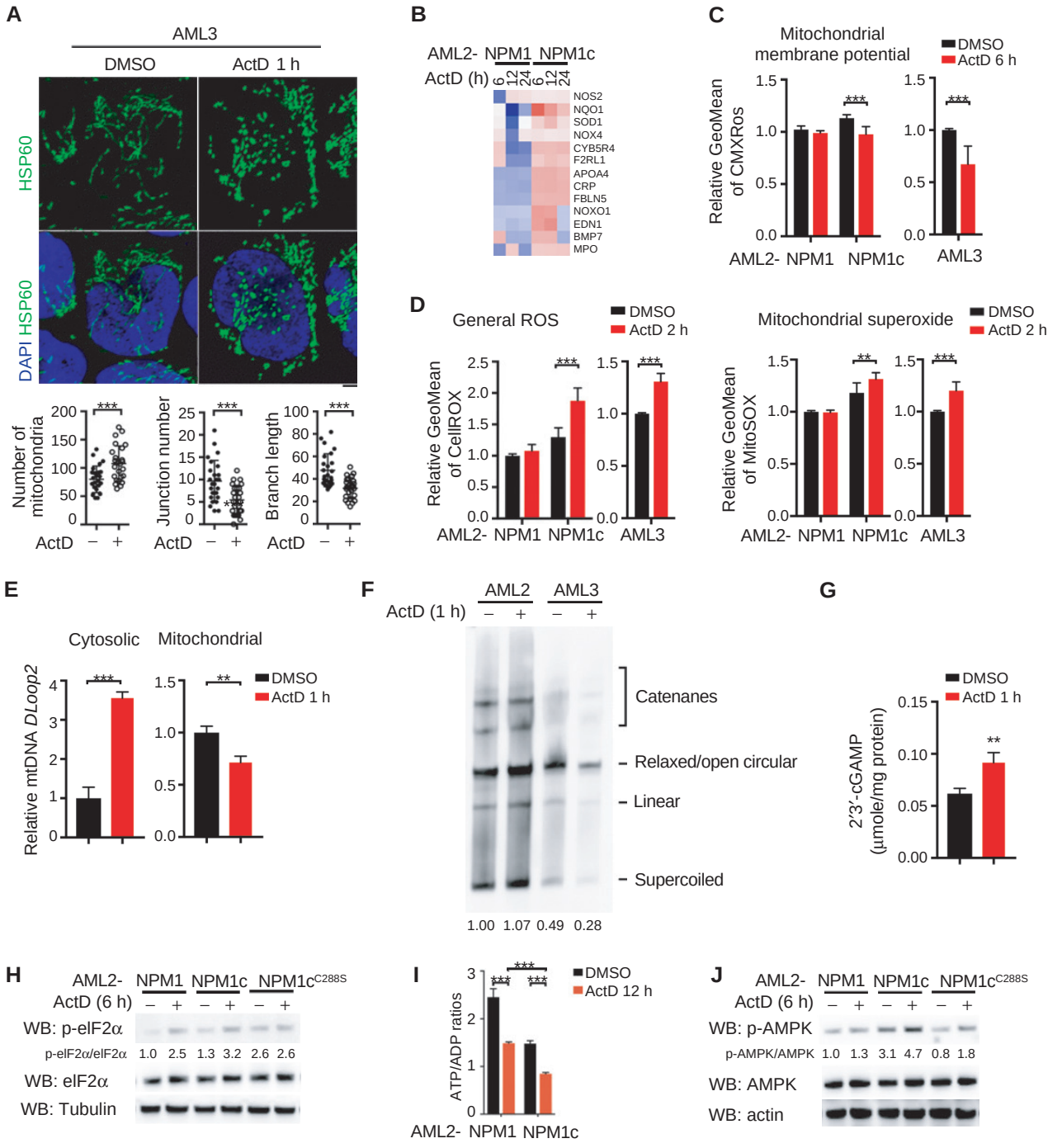

Figure 3. ActD targets mitochondria. **A,** Top, representative immunofluorescence analyses of mitochondrial morphology in AML3 cells treated with 5 nmol/L ActD. Bottom, mitochondrial fragmentation was quantified by number of mitochondria, of junction and branch length. The results are expressed as the mean value ± SD (error bars) of $n = 25$ cells per condition. Unpaired *t* test; ***, $P < 0.001$. Scale bar, 2 µm. **B,** Heat map (induction over mock-treated in the pool of samples) showing the expression of superoxide response genes upon ActD exposure. **C** and **D,** FACS analyses of mitochondrial membrane potential (**C**), ROS and mitochondrial superoxide production (**D**), after ActD exposure in AML2-derived isogenic cells. The results are expressed as the mean value ± SD. Unpaired *t* test. **, $P < 0.005$; ***, $P < 0.001$; $n = 3$. **E,** Effect of ActD on mtDNA abundance in the cytoplasm (left) or within mitochondria (right). Representative experiment of $n = 2$. **F,** Southern blot analysis of the different forms of mitochondrial DNA, in AML2 or AML3 cells treated or not with ActD (5 nmol/L) for 1 hour. **G,** levels of cytoplasmic cGAMP before or after ActD treatment. Representative experiment of $n = 2$. **H,** Western blot analyses of eIF2α and its phosphorylated form after ActD exposure. **I,** ATP/ADP ratio from metabolomic analyses of AML2 cell lines after ActD exposure. The results are expressed as the mean value of triplicate samples ± SD. Unpaired *t* test. ***, $P < 0.001$. **J,** Western blot analyses of AMPK and its phosphorylated form after ActD exposure.

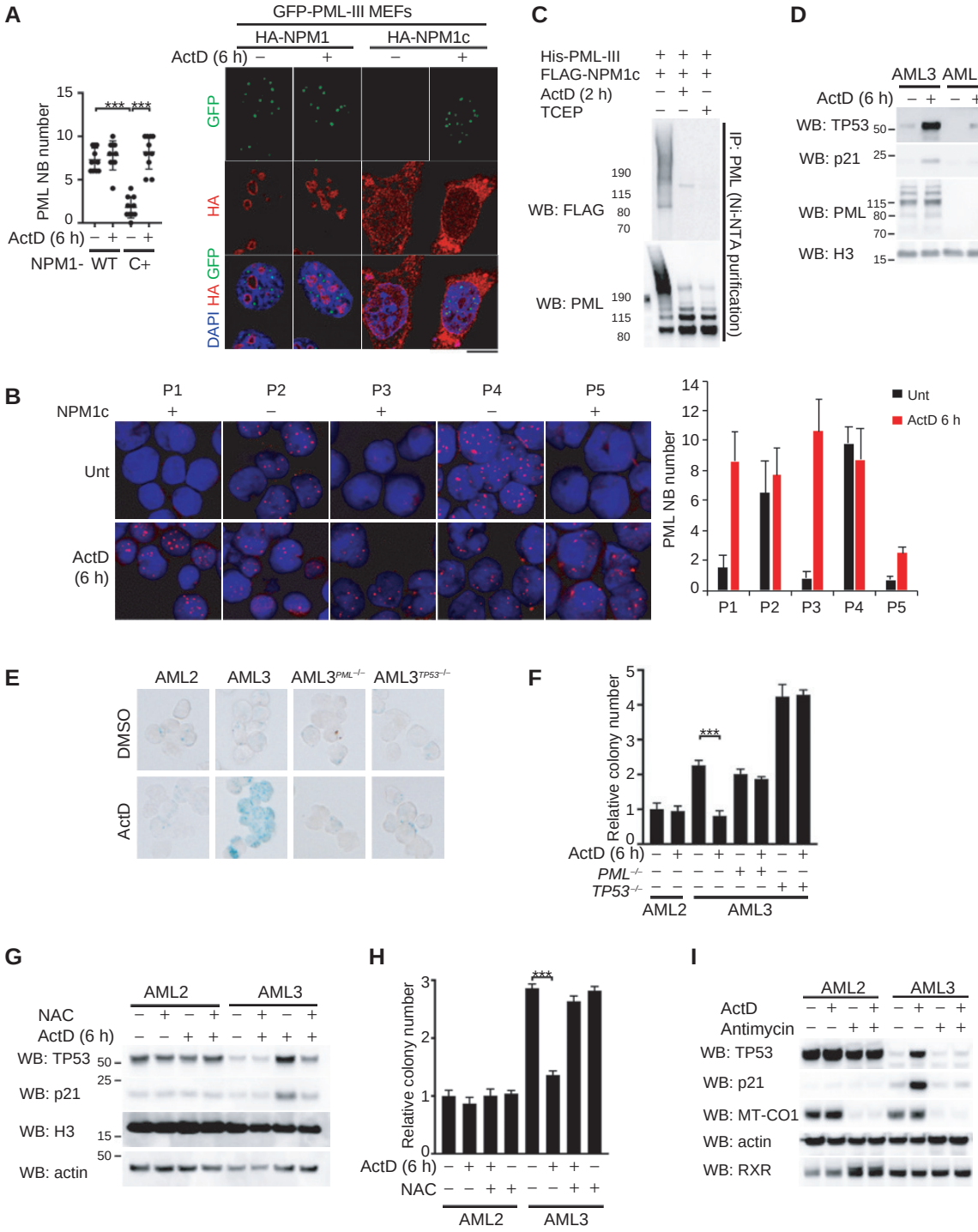

Figure 4. ActD activates a ROS/PML/TP53 senescence axis *ex vivo*. **A,** Quantification (left) and representative image (right) of PML NBs upon ActD exposure in MEFs stably expressing GFP-PML-III and transiently expressing NPM1 (WT) or NPM1c (C+). The results are expressed as the mean value ± SD (error bars) of $n = 10$ cells per condition. Unpaired *t* test; ***, $P < 0.001$. Scale bar, 10 μm. **B,** *Ex vivo* ActD treatment of primary AML blasts demonstrates PML NB restoration in NPM1c-AMLs. Representative images (left) and quantification (right). **C,** Histidine pulldown of disulfide-linked NPM1c-PML complex in transiently transfected 293T cells, before or after ActD exposure. **D,** Western blot analyses of AML3 and AML3$^{PML-/-}$ cells after ActD treatment. **E,** SA-β-gal staining of AML3 derivatives 7 days after 2 hours ActD pretreatment. **F,** Effect of ActD pretreatment on colony formation in the indicated AML cell lines. The results are expressed as the mean value of triplicate samples ± SD. Representative experiment of $n = 2$. Unpaired *t* test; ***, $P < 0.001$. **G,** Western blot analyses of NAC pretreated AML cells upon ActD exposure. **H,** Effect of NAC and ActD pretreatment on colony formation in the indicated AML cell lines. The results are expressed as the mean value of triplicate samples ± SD. Unpaired *t* test; ***, $P < 0.001$. Representative experiment of $n = 2$. **I,** Western blot analyses of ActD response of parental and mitochondria-depleted AML2 and AML3 cells. MT-CO1, Mitochondrial cytochrome *c* oxidase subunit 1; RXR, retinoid X receptor alpha.

mitochondrial clearance through mitophagy (37). Mitochondrial depletion abolished early ActD-triggered TP53 activation (Fig. 4I), suggestive for a key role of mitochondrial ROS in PML-dependent TP53 stabilization. Conversely, we used Thenoyl-trifluoroacetone (TTFA), a well-characterized inhibitor of mitochondrial complex II and major inducer of ROS (Supplementary Fig. S4E). In AML3 cells, TTFA decreased clonogenic activity in a PML-dependent manner (Supplementary Fig. S4F). In stable GFP-PML-III MEFs transiently expressing NPM1c, TTFA restored NB formation (Supplementary Fig. S4G). Collectively, these experiments establish the key role of mitochondrial ROS in ActD-driven activation of the PML NB-activated senescence checkpoint *ex vivo*.

ActD Exerts Leukemia-Specific Growth Suppression *In Vivo*

We first assessed ActD response in primary cells. We found no significant ability of low-dose ActD to promote TP53 stabilization in normal bone marrow progenitors *in vivo* or *ex vivo*, or in human or mouse primary fibroblasts (Supplementary Fig. S5A; ref. 35). In immunodeficient mice xenografted with primary human NPM1c-AML blasts, a 4-day course of ActD therapy significantly stabilized human TP53, but not mouse Trp53, highlighting tumor-specific targeting and implying that NPM1c sensitizes cells to ActD (Fig. 5A, top). ActD therapy inhibited leukemic growth and induced blast differentiation in that model (Fig. 5A, bottom). Similarly, in a murine NPM1c-driven AML model (38), ActD treatment again induced leukemia-selective Trp53 activation, AML regression, and blast differentiation (Fig. 5B). Finally, in AML3 xenografts, *PML* was required for TP53 activation and antileukemic effects of ActD (Fig. 5C). In contrast, ActD failed to cause regression of *MLL/ENL*–driven murine AMLs after 7 days (Supplementary Fig. S5B). Collectively, these *in vivo* observations suggest that ActD favors PML-dependent TP53 activation and regression of NPM1c-AMLs, but (at least initially) spares normal cells.

We then explored a NPM1c-AML patient who exhibited a 10^4-fold blast decrease 3 weeks after a 5-day course of single-agent ActD treatment, using the previously reported therapeutic scheme (refs. 21–23; Supplementary Fig. S5C). In leukemic blasts sequentially sampled from the peripheral blood of this patient during ActD treatment, the reformation of PML NBs was complete by 12 hours (Fig. 5D). Such ActD-induced NB reformation was accompanied by TP53 stabilization and target gene activation, including P21 (Fig. 5E and F). However, we failed to detect a significant increase in the L11/HDM2 interaction (Supplementary Fig. S3B) or γH2AX foci before 48 hours (Supplementary Fig. S5D, arrow), arguing against potent early activation of ribosomal and DNA-damaging checkpoints *in vivo*. Thus, PML NB reformation is an immediate response of AML cells to ActD therapy *in vivo*.

Pathway analyses of transcriptomes from AML-rich peripheral blood revealed activation of acute stress responses (expression of *HSP1A*, *FOS*, *EGR1*) and activation of PML NBs as early as 6 hours following initiation of therapy (Fig. 5G and H). We also observed immediate shutoff of NFκB targets, including extinction of IL8 expression, a distinct feature of mitochondrial dysfunction–driven senescence (ref. 37; Fig. 5H). We detected cGAS aggregation 6 hours after ActD treatment (Supplementary Fig. S5D). Despite daily ActD injections, these transcriptional changes were transient, pointing to the existence of adaptive control mechanisms (Fig. 5G). Nevertheless, ActD treatment triggered features of senescence (PML NBs, TP53 and P21 up, E2F down; Fig. 5E–H). Terminal deoxynucleotidyl transferase–mediated dUTP nick end labeling (TUNEL)–positive apoptotic cells were also detected 48 hours posttreatment (data not shown), indicating the cooccurrence of apoptosis.

A consolidation course of ActD treatment given when the patient had no residual leukemic blasts was not accompanied by major TP53 target activation or modulation of stress responses in normal blood cells (Fig. 5E; Supplementary Fig. S5E). Collectively, our findings support the idea that ActD-driven acute mitochondrial stress initiates PML NB–activated senescence/apoptosis in NPM1c AML cells *in vivo*.

ActD Potentiates Venetoclax Antileukemic Effects

In AML and myeloma cells, low basal complex II activity predicts venetoclax sensitivity (15, 39). Having demonstrated NPM1c-driven complex II impairment (Supplementary Fig. S2E–S2G) and ActD-mediated mitochondrial toxicity (Fig. 3), we hypothesized that ActD might enhance the established anti-AML clinical activity of venetoclax (40, 41). Venetoclax induced mitochondrial fragmentation, reduction of mitochondrial membrane potential, production of ROS, and leakage of mtDNA to the cytoplasm of AML3 cells (Fig. 6A–E). Critically, all of these features were strongly potentiated by cotreatment with ActD. In AML2-NPM1c (but not AML2-NPM1), venetoclax and ActD strongly synergized to activate cGAS activity (Fig. 6F) and PML NB reformation (Supplementary Fig. S6A). A brief pretreatment with both drugs abolished clonogenic growth of NPM1c-expressing cells, only in the presence of PML (Fig. 6G). Accordingly, in AML3 xenograft models, venetoclax and ActD strongly synergized to extend survival, an effect that also requires PML (Fig. 6H).

We then explored the ActD–venetoclax interaction in three other NPM1c-driven AML models *in vivo*. First, in murine

Figure 5. ActD exerts AML-specific growth suppression *in vivo*. **A,** Top, TP53 or HDM2 stabilization in bone marrow of immunodeficient mice xenografted with primary patient NPM1c-AML cells. +, *Ex vivo MLL/ENL* ActD-treated cells for 3 hours, as a positive control. Bottom, AML features in this mouse model following treated or not with ActD for 5 days. Unpaired *t* test. *, $P < 0.05$; **, $P < 0.005$; ***, $P < 0.001$. Representative experiment of $n = 3$. **B,** Top, Trp53 stabilization in CD45.2$^+$ NPM1c-driven murine AML blasts versus CD45.2$^-$ normal mouse cells upon ActD exposure. Bottom, AML features after a week of ActD therapy. The results are expressed as the mean value ± SD. Unpaired *t* test. *, $P < 0.05$; **, $P < 0.005$; ***, $P < 0.001$. Representative experiment of $n = 3$. **C,** Western blot analyses of AML3 and AML3$^{PML-/-}$ engrafted immunodeficient mice treated or untreated with ActD for a week (left) and percentage of CD45$^+$ AML3 blasts in the bone marrow (right). Unpaired *t* test. ***, $P < 0.001$. $n = 2$. **D,** Top, immunofluorescence analyses of blast-rich blood samples from an AML patient during ActD therapy. Bottom, quantification of PML NBs. Scale bar, 10 μm. **E,** Heat map of upregulated TP53 target genes in AML cells from ActD-treated patient. **F,** Western blot analyses of AML-rich blood samples during the first cycle of ActD therapy. **G,** GSEAs of differentially expressed genes in the patient treated with ActD. **H,** Expression of NFκB targets (left), acute stress response (middle), and proliferation genes (right) in AML-rich peripheral blood from patient during therapy (data from the microarray experiments).

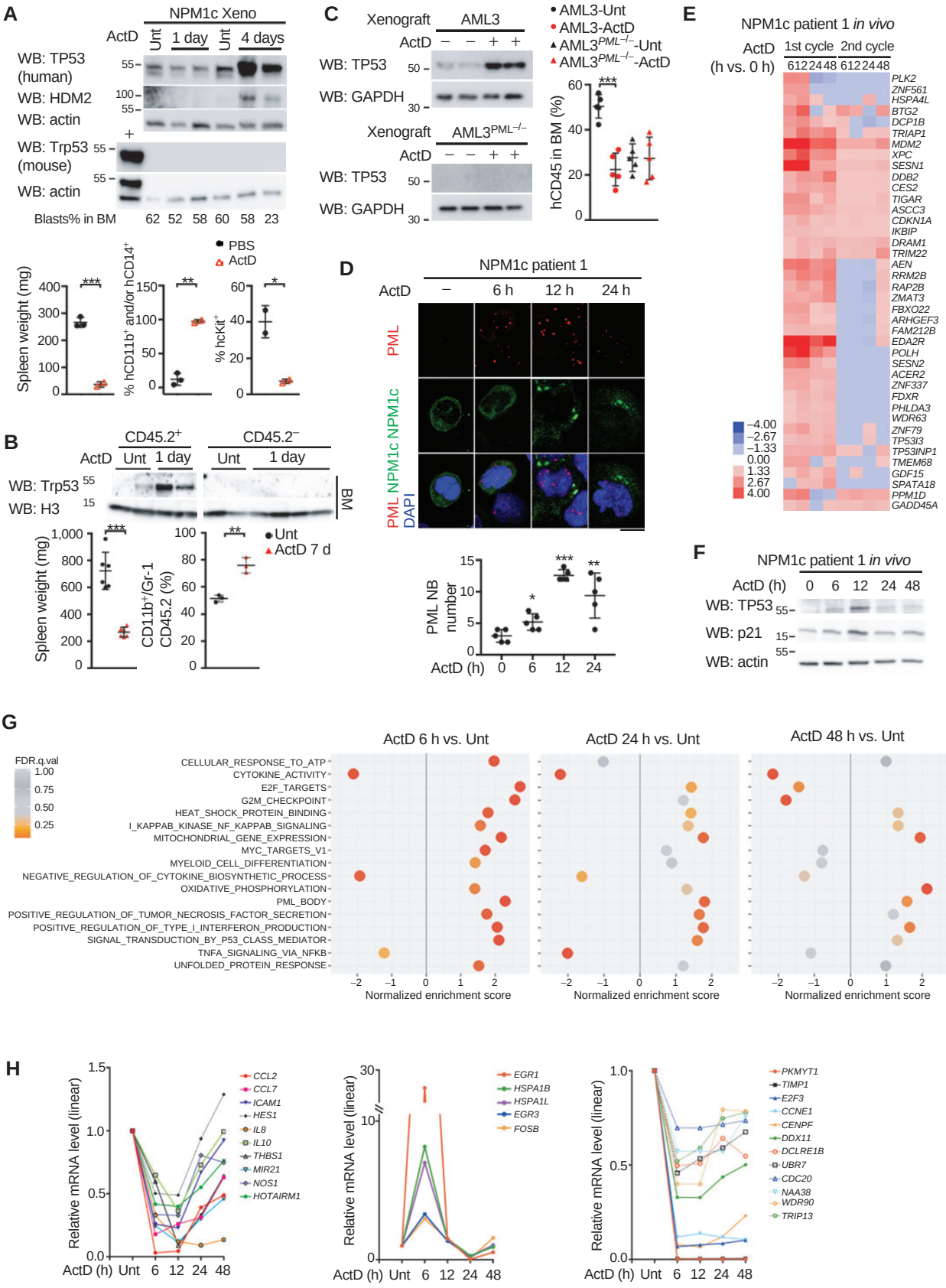

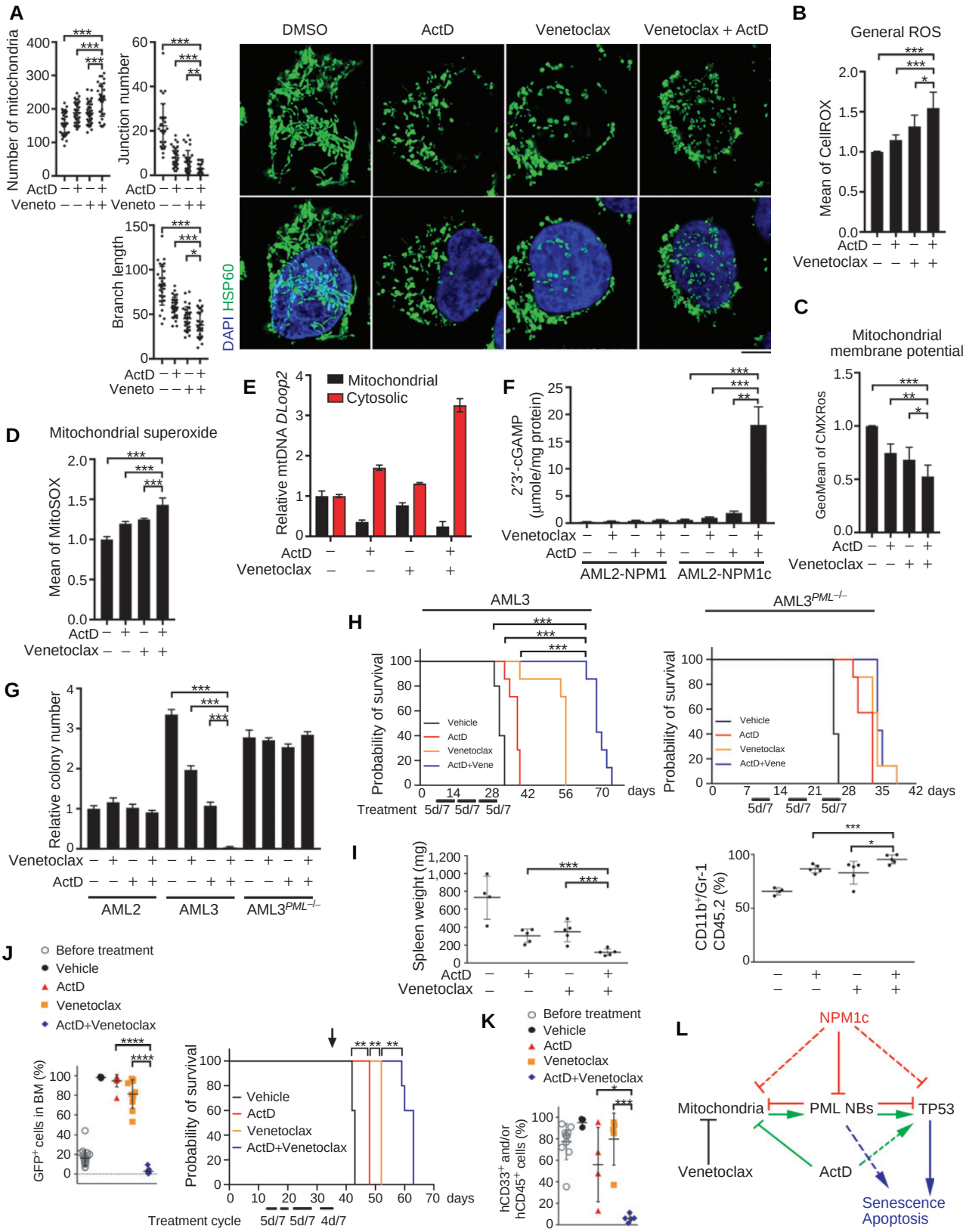

NPM1c-driven AMLs (38), the combination treatment dramatically decreased leukemic burden and enhanced blast differentiation (Fig. 6I). Second, in a double conditional knock-in of NPM1c plus IDH1^{R132H} (ref. 42; to be fully described elsewhere), only the combined treatment eliminated AML cells from the bone marrow and yielded a significant survival advantage (Fig. 6J). Finally, in xenografted primary AML blasts, ActD and venetoclax (but neither agent alone) cleared AML cells from the bone marrow (Fig. 6K). Collectively, the ActD–venetoclax combination synergizes for mitochondrial targeting, yields PML-dependent growth arrest, and clears leukemia in several distinct *in vivo* AML models.

DISCUSSION

NPM1c expression alters PML NB formation in multiple cell types, including normal HSCs *in vivo*. NPM1c is an abundant protein that may impede NB biogenesis through direct PML binding and sequestration, degradation, or indirect control of PML oxidation, which drives NB formation (4, 43). PML is critical for mitochondrial fitness (9–11, 44). NPM1c-induced mitochondrial defects reflect, at least in part, NB disruption, because NPM1c expression in *Pml*$^{-/-}$ mESCs did not further aggravate the prominent mitochondrial morphologic alterations resulting from PML loss (Supplementary Fig. S2K). Functionally, NPM1c-mediated NB impairment and mitochondrial defects, which drive the integrated stress response, may all contribute to the transformation of *DNMT3A*- or *IDH1/2*-immortalized stem cells into full-blown leukemia (2, 12, 26), through cell-autonomous mechanisms (including ROS signaling and impaired senescence) and/or inflammation-mediated remodeling of the microenvironment (45, 46).

Targeting mitochondrial function by antibiotics was proposed as a therapeutic option for cancer (19). Low-dose ActD can induce reversible cell-cycle arrest, without DNA damage or apoptosis (35) and accordingly was well tolerated by nonleukemic primary cells *ex vivo* or *in vivo* (Fig. 5). In contrast, ActD triggers rapid, but transient, alterations in NPM1c-primed mitochondria (Fig. 3A; Supplementary Fig. S3D). ActD also induces mtDNA leakage to the cytoplasm (Fig. 3E) possibly caused by ActD intercalation within the mitochondrial genome. Such mtDNA release, followed by activation of cGAS, and its downstream IFN pathway could activate senescence, as well as antileukemic immune responses (31, 36, 47, 48). Besides cGAS activation, ActD induces ROS, which are required for ActD-induced senescence *ex vivo* through PML NB reformation and TP53 activation (Figs. 4 and 6L; refs. 4, 5, 43). The actual origin of these ROS remains poorly characterized. Upon mitochondrial stress, complex II, at the junction between the TCA cycle and the ETC, which is highly expressed in Lin-ScaI+cKit+ (LSK) progenitors (49), regulated by PML (50) and by NPM1c (Supplementary Fig. S2F and S2G), could play a role in ROS production, as the complex II inhibitor TTFA mimics ActD in NPM1c-expressing cells *ex vivo* (Supplementary Fig. S4E–S4G). Our *ex vivo* observations suggest that a significant part of ActD activity is mediated through mitochondrial ROS, PML NB reformation, and TP53 activation. In the ActD-treated patient with AML, we also found some evidence for mitochondria dysfunction–induced senescence (37). Later, ActD intercalation into nuclear DNA, inhibition of RNA Pol I activity, and activation of the ribosomal checkpoint (34) could also contribute to ActD therapeutic activity. NPM1c-driven PML NB disruption and their ActD-induced reformation (Figs. 5D and 6K) evoke a striking, but unexpected, similarity with APL treatment by retinoic acid and arsenic (6). PML NBs may thus emerge as key hubs inactivated by oncogenes (*NPM1c*, *PML/RARA*), but reactivated by antitumor drugs (retinoic acid, arsenic, ActD, or IFNα; ref. 51). Actually, in an APL mouse model, an ETC inhibitor drove prolonged remissions (52), possibly reflecting mitochondrial ROS-induced PML NB restoration. This ROS/PML/TP53 cascade may also promote ActD responses in non-NPM1c-AMLs harboring dysfunctional mitochondria. Doxorubicin similarly fragments mitochondria of NPM1c-expressing cells to drive ROS-induced TP53 activation (Supplementary Fig. S6B–S6D), suggesting that dual targeting of nucleus and mitochondria may be shared by other antitumor antibiotics.

High mitochondrial ETC or OXPHOS activities were repeatedly linked to venetoclax or chemotherapy resistance in AML (13–15, 17) or other cancers (18). Conversely, inhibition of mitochondrial translation sensitizes AML cells to venetoclax (16). Thus, the NPM1c-associated defects in mitochondrial function unraveled here likely underlie the favorable prognosis of NPM1c-AMLs. Finally, ActD and venetoclax exert synergistic effects to clear NPM1c-AMLs in multiple *in vivo* models (Fig. 6). Clinically supporting our observations, ActD was very recently proposed to circumvent venetoclax resistance in salvage therapy of multi-relapsed patients with AML (53). Thus, mechanism-based prospective trials associating ActD and venetoclax could be envisioned in patients with AML.

Figure 6. ActD enhances Venetoclax antileukemic effects. **A,** Mitochondrial morphology in AML3 cells treated with 5 nmol/L ActD and/or 1 μmol/L venetoclax for 3 hours. Left, mitochondrial fragmentation was quantified by number of mitochondria, of junction and branch length. Right, immunofluorescence analysis of mitochondrial morphology. The results are expressed as the mean value ± SD of $n = 30$ cells per condition. Unpaired *t* test. *, $P < 0.05$; **, $P < 0.005$; ***, $P < 0.001$. Scale bar, 5 μm. **B–D,** FACS analyses of general ROS (**B**), mitochondrial membrane potential (**C**), and mitochondrial superoxide production (**D**), after ActD and/or venetoclax exposure in AML3 cells. Cell were treated with indicated drugs for 3 hours in **B** and **D** and 6 hours in **C**. The results are expressed as the mean value ± SD from from $n = 2$ experiments. Unpaired *t* test. ***, $P < 0.001$. **E,** Leakage of mitochondrial DNA to the cytoplasm in response to a 3-hour ActD or venetoclax exposure in AML3 cells. Results are expressed as the mean value of triplicate samples ± SD. Unpaired *t* test. ***, $P < 0.001$. Representative experiment of $n = 2$. **F,** 2′3-cGAMP concentration in AML cells after 6 hours exposure to venetoclax and/or ActD. Representative experiment of $n = 2$. **G,** Methylcellulose colony formation assays of AML cell lines upon 2 hours preseeding exposure to venetoclax and/or ActD. Results are expressed as the mean value of triplicate samples ± SD. Unpaired *t* test. ***, $P < 0.001$. Representative experiment of $n = 3$. **H,** Survival of immunodeficient mice xenografted with AML3 or AML3$^{PML-/-}$ cells and treated with ActD or venetoclax, 5 days per week. **I,** AML features in NPM1c-driven AML mice treated with ActD and or not venetoclax for 5 days. The results are expressed as the mean value ± SD. Unpaired *t* test. *, $P < 0.05$; ***, $P < 0.001$. $n = 2$. **J,** Response to ActD and/or venetoclax in a transplantable AML model initiated by NPM1c + IDH1^{R132H} mutation. Left, GFP abundance in bone marrow samples collected at treatment interruption (arrow in the survival curve, right), Representative experiment of $n = 3$. **K,** Abundance of human AML cells in xenografted mice treated for two weeks. Combined therapy induces AML regression. **L,** Model of venetoclax/ActD/mitochondria/PML/TP53 interplays in NPM1c-AMLs. Dashed lines point to likely mechanisms not directly explored here.

METHODS

Cell Lines

Human AML cell lines were maintained in minimum essential medium-alpha plus GlutaMAX (Thermo Fisher Scientific; catalog no. 32561094) supplemented with 20% FBS in the presence of 100 U/mL of penicillin, 100 μg/mL of streptomycin, and were incubated at 37°C with 5% CO_2 (see key resource table for all details). To establish isogenic NPM1c-expressing AML2 cells, cells were transduced with a lentivirus expressing FLAG-GFP–tagged NPM1, NPM1c, or NPM1c-C288S and selected for GFP expression by FACS. WI38 cells were maintained in Eagle MEM (ATCC; catalog no. 30–2003) supplemented with 10% FBS in the presence of 100 U/mL of penicillin and 100 μg/mL of streptomycin. Primary MEFs were obtained from E18 mouse embryos and maintained in DMEM plus GlutaMAX (Thermo Fisher Scientific; catalog no. 41965062) supplemented with 10% FBS, 1× nonessential amino acids solution, 100 U/mL of penicillin, and 100 μg/mL of streptomycin. Normal CD34-positive cells were purified by using Dynabeads CD34 Positive Isolation Kit (Thermo Fisher Scientific; catalog no. 11301D). mESC line E14 was maintained on gelatin-coated dishes and cultured in DMEM supplemented with 10% FBS, 1,000 U/mL leukemia inhibitory factor, 50 U/mL penicillin, 50 μg/mL streptomycin, 2 mmol/L GlutaMAX, 0.1 mmol/L nonessential amino acids, 1 mmol/L sodium pyruvate, and 0.1 mmol/L 2-mercaptoethanol. The medium was changed every other day. All cell lines were repeatedly shown to be *Mycoplasma* negative by PCR testing (Eurofins). OCI-AML2 and OCI-AML3 were obtained from DSMZ, regularly authenticated by NPM1c expression, and genetically modified in house. Details on *PML* and *TP53* inactivation by CRISPR in AML3 cells or NPM1c CRISPR in mESCs can be found in the Supplementary Materials and Methods. mESCs were obtained from P. Thérizol (INSERM U944), primary and SV40-immortalized MEFs were derived in house. AML2-NPM1c and AML2-NPM1 cells were regularly flow-sorted to ensure continuous GFP expression. ActD, NAC, glutathione monoethyl ester (GSH-MEE), antimycin A, and doxorubicin were purchased from Sigma (catalog nos. 01815, A7250, G1404, A8674, D1515). Human cGAS inhibitor G140 was purchased from InvivoGen (catalog no. inh-g140).

AML Patient Samples

The study was conducted according to the Declaration of Helsinki and approved by our institutional ethics committee. Primary AML cells were obtained upon written informed consent from the patient during the off-label study. Human primary AML cells were isolated by density gradient centrifugation of either peripheral blood or bone marrow. AML was defined as *NPM1*-mutated on the basis of targeted sequencing analysis.

Animal Studies

For the NPM1c leukemia mouse model, C57BI6-CD45.1 mice were irradiated with 4.5 Gy and then engrafted with 10^6 CD45.2-NPM1c leukemic cells, a kind gift from P.G. Pelicci of the Instituto Europeo di Oncologia (38). In the experiment shown in Fig. 5B, mice were intraperitoneally injected with ActD (60 μg/kg/day) 19 days after engraftment and sacrificed 24 hours later after an additional ActD injection 1 hour before euthanasia. $CD45.2^+$ bone marrow cells were sorted by FACS (ARIA2, Becton Dickinson) and lysed directly by Laemmli buffer containing 20 mmol/L NEM and 10% 2-mercaptoethanol, followed by Western blot analysis. For the spleen weight or cytometric analyses, mice were intraperitoneally injected daily with ActD (60 μg/kg/day) for 7 or 10 days after engraftment. CD45.2 and differentiation markers Mac-1/Gr-1 triple-positive cells were examined by FACS. In the experiment shown in Fig. 6H, 10 days after engraftment, mice were intraperitoneally injected with ActD (60 μg/kg/day) and/or orally fed with venetoclax (INTERCHIM; catalog no. 3 × 552A) daily for 5 days. Vehicle (60% Phosal 50 PG, 30% PEG400, 10% ethanol) was administered as control. Mice were sacrificed after an additional day without treatment. Spleen weights were measured and percentages of CD45.2 and differentiation markers Mac-1/Gr-1 triple-positive cells were analyzed using FACS.

For the patient-derived xenografts, shown in Fig. 5A (top), 10 to 12 week-old NOD/SCID gamma SGM3 (NSGS) mice were treated with busulfan (Busilvex, 20 mg/kg) followed 24 hours later by engraftment of 9×10^4 NPM1c-AML patient mononuclear cells (NPM1c/FLT3 wt). Seventy-two days later, mice were treated daily with ActD (60 μg/kg/day) for 1 or 4 days and sacrificed for bone marrow cells.In the experiment shown in Fig. 5A (bottom), NSGS mice were irradiated with 1.5 Gy 24 hours before engraftment of 2.85×10^5 AML patient mononuclear cells. Eighty-seven days later, mice received the first intravenous injection with PBS or ActD (120 μg/kg/day) and then were treated daily for 4 more days by intraperitoneal injection, followed by 2 days without any further treatment prior to sacrifice. Percentage of human $CD33^+$ and/or $CD45^+$ and KIT^+ bone marrow cells were analyzed using FACS. In the experiment shown in Fig. 6J, 5 to 10-week-old NSGS mice were preconditioned by 1.25 Gy irradiation, followed by engraftment of 1×10^6 NPM1c-AML patient mononuclear cells. Thirty-five days later, mice were ActD-treated (60 μg/kg/day) and/or venetoclax-treated (100 mg/kg/day) daily 5 days per week for 2 weeks. Percentage of human $CD33^+$ and/or $CD45^+$ bone marrow cells was analyzed using FACS by intrabone aspiration 5 days before and 15 days after starting the treatment.

For the NPM1c/$IDH1^{R132H}$ GFP^+ leukemia mouse model, C57BL/6 mice were irradiated with 4.5 Gy and then engrafted with 10^6 AML cells, a kind gift from T.W. Mak. Thirteen days after engraftment, mice were intraperitoneally injected with ActD (60 μg/kg/day) and/or fed by venetoclax (100 mg/kg/day) daily, 4 or 5 days per week. Percentage of GFP^+ bone marrow cells was analyzed using FACS by intrabone aspiration 3 days before and 16 days after starting the treatment. Mice were then followed until they reach humane endpoints and then euthanized.

For the experiment shown in Figs. 5C and 6H, NSGS mice were treated with Busulfan (Busilvex; 20 mg/kg) for 24 hours, followed by engraftment of 10^6 AML3 derivatives for 7 days. Mice were intraperitoneally injected with ActD (60 μg/kg/day) for 4 weeks (5 days per week; Fig. 5C) or 3 weeks (Fig. 6H). Human $CD45^+$ bone marrow cells were examined by FACS and Western blot analysis.

For the experiments shown in Figs. 1A, 2A, and Supplementary Fig. S2A, LSK fraction was sorted and stained as described previously (49) from $NPM1c^{A/+}$ and control mice (26) 4 weeks after tamoxifen injection. Briefly, committed hematopoietic cells were depleted through MACS LS column (Miltenyi Biotec) and FLSK cells were sorted by FACS using the following antibodies: CD3e-biotin, CD8-biotin, IgM-biotin (Life Technologies; catalog no. 553728, catalog nos. 13–0081–85 and 13–5790–85), CD4-biotin, B220-biotin, Mac1-biotin, Tert119-biotin, CD19-biotin, Nk1.1-biotin (BD Biosciences; catalog nos. 553728, 553086, 553309, 553672, 553784, 553163), Gr1-biotin, CD150-perCp/Cy5.5, c-kit-APC/Cy7 (BioLegend; catalog nos. 108404, 115922, 105826), Il7Ra-biotin, CD135-biotin, streptavidin-Pacific Blue, Sca1-PE/Cy7, CD48-APC (eBioscience; catalog nos. 13–1271–85, 13–1351–82, 48–4317–82, 25–5981–81, 17–0481–82). FLSK cells were resuspended in 20 μL of StemSPAN SFEM (StemCell Technologies; catalog no. 9600), then seeded on Lab-Tek II Chamber Slide (Thermo Fisher Scientific; catalog no. 154453) coated with Retronectin (ClonTech; catalog no. T202). Rabbit polyclonal anti-TOM20 (Santa Cruz Biotechnology; catalog no. FL-145, dilution 1:100), mouse monoclonal anti-B23 (Sigma-Aldrich; catalog no. B0556, dilution 1:100), and mouse monoclonal anti-PML (Millipore Sigma; catalog no. MAB3738, clone 36.1–104, dilution 1:100) were used for the detection. Z-stack values were acquired on a Leica SP5, then deconvolved using the Richardson–Lucy algorithm using measured point spread function. Representative iso-surface images and the analysis of number and volume of objects were obtained by Imaris 7 (Bitplane).

All experiments in mice were performed in accordance with protocols approved by the Comités d'éthique en Expérimentation Animale Paris-Nord no. 121 (project no. 20710–2019071616338948 v2). For the mouse NPM1c leukemia model, C57BL/6-CD45.1, mice were purchased from Charles River Laboratories (agreement no. C 69 208 1301) at 6 weeks old and kept under specific pathogen–free (SPF) conditions. For OCI-AML3 or primary patient blasts xenograft experiment, NOD/Shi-*scid IL2rγ*$^{-/-}$ (NSG) mice were obtained from Jackson Laboratories and kept in SPF conditions.

Immunoprecipitation Analyses

For immunoprecipitation analysis, cell extraction was performed with RIPA lysis buffer containing 50 mmol/L Tris (pH 8.0), 0.15 mol/L NaCl, 1% NP40, 1% sodium deoxycholate, 0.1% SDS, 1 mmol/L phenylmethylsulfonylfluoride, 1 μg/mL aprotinin, and 1 μg/mL leupeptin, 10 mmol/L NEM. Equal amounts of protein lysates were used for immunoprecipitation with indicated antibodies. For protein expression analysis, cells were collected, counted, and lysed in XT sample buffer (Bio-Rad) or 2x Laemmli buffer both containing 20 mmol/L NEM and 10% 2-mercaptoethanol. Samples were heated at 95°C for 10 minutes. For disulfide-mediated PML–NPM1c complexes, protein samples were divided into two equal aliquots with XT sample buffer containing 20 mmol/L NEM. One of the aliquots was freshly added disulfide bond breaker tris-(2-carboxyethyl) phosphine (TCEP; Thermo Fisher Scientific) and heated at 95°C for 5 minutes. Details on immunodetection in precipitation sample and cell lysate can be found in Supplementary Materials and Methods.

Mitochondrial Explorations

Mitochondrial superoxide, membrane potential, and mass were measured by using MitoSOX, MitoTracker CMXRos, and MitoTracker red FM probes (Thermo Fisher Scientific; catalog nos. M36008, M7512, M22425), respectively. Live-cell labeling was done according to manufacturer's instructions and analysis made by FACS (FACSCalibur, BD Biosciences).

To measure relative mitochondrial gene expression by reverse transcriptase PCR, whole-cell RNA was isolated using RNeasy Mini Kit (Qiagen; catalog no. 74104). Reverse transcription was performed using iSCRIPT cDNA Synthesis Kit following the manufacturer's instructions (Bio-Rad). Quantitative real-time PCR analysis was performed using Roche LightCycler 480 system with SYBR Green PCR Master Kit (Roche). Primers are listed in Supplementary Material Methods.

Cytosolic/mitochondria resident mtDNA extraction was carried out as described previously (36). Briefly, 15×10^6 mESCs or 10×10^6 AML cells were washed with ice-cold PBS and permeabilized by digitonin buffer containing 150 mmol/L NaCl, 50 mmol/L HEPES (pH 7.4), 1 mol/L Hexylene glycol, and 25 μg/mL digitonin for 10 minutes at 4°C, then centrifuged at $2{,}000 \times g$ for 15 minutes. The cytosolic supernatants were transferred to fresh tubes and spun at 12,000 rpm for 10 minutes to remove any remaining cellular debris, yielding cytosolic preparations free of nuclear, mitochondrial, and any other organelles. Cytosolic DNA was purified by using QIAquick Nucleotide Removal Kit (QIAGEN; catalog no. 28304). The intact cell pellets were resuspended in 50 μmol/L NaOH and boiled for 30 minutes to solubilize DNA. Fifty microliters of 1 mol/L Tris-HCl pH 8.0 was added to neutralize the pH. Mitochondria and nuclear DNA were purified by using QIAamp DNA Mini Kit (QIAGEN; catalog no. 51304). Primers are listed in in Supplementary Materials and Methods. mtDNA was analyzed by Southern blotting. Briefly, 1 μg of mitochondria DNA was separated over a 0.5% agarose gel overnight in TAE, blotted by capillary transfer onto Hybond-N+ membranes (GE Healthcare). The mtDNA was visualized by Southern blotting using a probe against nucleotide positions 168–604 of human mtDNA labeled using digoxigenin-labeled nucleotide (PCR DIG Probe Synthesis Kit; Sigma-Aldrich; catalog no. 11636090910) and later revealed using anti-digoxigenin antibodies.

To measure 2′3-cGAMP, 40×10^6 AML cells were washed with ice-cold PBS and lysed by M-PER extraction reagent (Thermo Fisher Scientific; catalog no. 78501). 2′3′-cGAMP were quantified by an ELISA Kit (Cayman; catalog no. 501700), which is based on the competition between 2′3′-cGAMP and a 2′3′-cGAMP–horseradish peroxidase conjugate for a limited amount of 2′3′-cGAMP polyclonal antiserum.

Microarray Analysis

Whole-cell RNA from one million cells of AML derivates or peripheral blood mononuclear cells of patient were purified using RNeasy Mini Kit (QIAGEN). Microarray were performed at the core facility of Institut de Recherche Saint Louis of Université de Paris (Paris, France). Details can be found in Supplementary Materials and Methods. Primary data are accessible in ArrayExpress (accession ID: E-MTAB-10397). The mass spectrometry proteomics data have been deposited to the ProteomeXchange Consortium via the PRIDE partner repository with the dataset identifier PXD025507.

Transmission Electron Microscopy

AML2-derived cell lines were washed and fixed in 1.6% glutaraldehyde in 0.1 mol/L phosphate buffer. Cell pellets were secondary fixed with 2% osmium tetroxide and dehydrated using ethanol. Cells were embedded in Epon 812. Ultrathin sections and then stained with standard uranyl acetate and lead citrate solutions. Mitochondrial morphology was analyzed using FEI Tecnai 12 electron microscopy equipped with SIS Mega view III CCD camera.

Gene Set Enrichment Analysis

For the experiment shown in Figs. 1H and 5G, gene set enrichment analysis (GSEA) was performed using Hallmarks (h.all.v7.1), Gene ontology (c5.all.v7.1), or Curated (c2.cp.KEGG) gene set. 371 genes were selected on the basis of GSEA Hallmarks gene set (h.all.v7.1). For the experiment shown in Supplementary Fig. S2B, GSEA was performed using Gene ontology (c5.all.v7.1) or Curated (c2.cp.KEGG) gene set.

Statistical Analysis

GraphPad Prism software was used to perform multiple unpaired two-tailed *t* test to determine the *P* values and look for significant changes in the data generated from the isogenic cell lines and different drug treatment *in vivo* or *ex vivo*. All data are expressed as mean ± SD of technical replicates from a representative experiment of the performed ones, as indicated. For all graphs, *, $P = 0.01$–0.05; **, $P = 0.001$–0.01; ***, $P < 0.001$. For the experiment shown in Supplementary Fig. S3F, ROS and inflammation-related gene changes from AML2-expressing NPM1c versus NPM1 or AML2-expressing NPM1 treated with ActD versus DMSO were selected to perform linear regression analysis using GraphPad Prism software.

Authors' Disclosures

L. Adès reports consulting or advisory roles for BMS/Celgene and AbbVie and research funding from BMS/Celgene. R. Itzykson has received honoraria from AbbVie, Amgen, Astellas, BMS-Celgene, Daiichi-Sankyo, Jazz Pharmaceuticals, Karyopharm, Servier, and Stemline, and research funding from Janssen, Novartis, and Oncoethix (now Merck SD). A. Bazarbachi is on the speaker bureau or advisory board of Novartis, Roche, Sanofi, Jazz, Adienne, Astellas, Takeda, Hikma, Celgene, Janssen, MSD, AbbVie, Pfizer, and Amgen. B. Falini licensed a patent on NPM1 mutants (n. 102004901256449). B. Falini and M.P. Martelli declare honoraria from Rasna Therapeutics, Inc for scientific advisor activities. M.P. Martelli also declares consultancy at scientific advisory boards for AbbVie, Amgen, Celgene, Janssen, Novartis, Pfizer, and Jazz Pharmaceuticals, and honoraria from Amgen, Celgene, Janssen, and Novartis. L. Brunetti declares consultancy at scientific advisory boards for AbbVie. Other authors have nothing to disclose.

Authors' Contributions

H. Wu: Data curation, formal analysis, investigation. **D. Rérolle:** Data curation, investigation. **C. Berthier:** Investigation. **R. Hleihel:** Investigation. **T. Sakamoto:** Resources. **S. Quentin:** Investigation. **S. Benhenda:** Resources. **C. Morganti:** Resources, investigation. **C. Wu:** Investigation. **L. Conte:** Investigation. **S. Rimsky:** Methodology. **M. Sebert:** Resources. **E. Clappier:** Resources. **S. Souquere:** Investigation. **S. Gachet:** Resources, investigation. **J. Soulier:** Resources. **S. Durand:** Formal analysis. **J.J. Trowbridge:** Resources. **P. Benit:** Investigation. **P. Rustin:** Investigation. **H. El Hajj:** Validation. **E. Raffoux:** Resources. **L. Ades:** Resources. **R. Itzykson:** Resources. **H. Dombret:** Resources. **P. Fenaux:** Resources. **O. Espeli:** Methodology. **G. Kroemer:** Methodology. **L. Brunetti:** Resources. **T.W. Mak:** Resources. **V. Lallemand-Breitenbach:** Conceptualization. **A. Bazarbachi:** Conceptualization. **B. Falini:** Conceptualization. **K. Ito:** Resources, investigation. **M. Martelli:** Conceptualization. **H. de Thé:** Conceptualization, resources, data curation, formal analysis, supervision, writing–original draft.

Acknowledgments

We warmly thank P.G. Pelicci for sharing mouse leukemia models, V. Montcuquet for the animal husbandry, N. Setterblad and S. Duchez for the imaging and cytometry platforms, C. Vallot for bioinformatic advice, C. Bally for help with the patient samples, the 3P5 proteomic facility of Institut Cochin, the imaging ORION platform of Collège de France for decisive help in PML NBs and mitochondrial alteration quantification, A. Mourier for discussions and advice, A. Rötig for DNA of mitochondria-depleted cells, M.H. Verlhac, E. Gilson, U. Sahin, J. Ablain, R. Rodriguez, C. Esnault, and other lab members for advice and comments on the manuscript. This work is dedicated to the first author's late father Jung-Mao Wu and all those loved ones lost to COVID-19. Work in the Paris laboratories is supported by Collège de France, INSERM, CNRS, University de Paris and University PSL, INCA [CAMELIA project, TRANSCAN (DRAMA project) and PLBIO19-198], Fondation du Collège de France and Fonds Saint Michel, and the Sjöberg Award (to H. de Thé). This project has received funding from the European Research Council (ERC) under the European Union Horizon 2020 research and innovation program (Grant agreement n° 785917, PML-THERAPY). C. Morganti is supported by NYSTEM Einstein Training Program in Stem Cell Research. K. Ito and J.J. Trowbridge are supported by NIH grants, and K. Ito is a Leukemia Lymphoma Society Scholar. Work in Beyrouth and Perugia is supported by ERC grants (785917, 740230, 725725) and the ARC Foundation for Cancer Research (Leopold Griffuel Prize to B. Falini).

The publication costs of this article were defrayed in part by the payment of publication fees. Therefore, and solely to indicate this fact, this article is hereby marked "advertisement" in accordance with 18 USC section 1734.

Note

Supplementary data for this article are available at Cancer Discovery Online (http://cancerdiscovery.aacrjournals.org/).

Received February 8, 2021; revised May 7, 2021; accepted July 21, 2021; published first July 23, 2021.

REFERENCES

1. Falini B, Brunetti L, Sportoletti P, Martelli MP. NPM1-mutated acute myeloid leukemia: from bench to bedside. Blood 2020;136:1707–21.
2. Shlush LI, Zandi S, Mitchell A, Chen WC, Brandwein JM, Gupta V, et al. Identification of pre-leukaemic haematopoietic stem cells in acute leukaemia. Nature 2014;506:328–33.
3. Brunetti L, Gundry MC, Sorcini D, Guzman AG, Huang YH, Ramabadran R, et al. Mutant NPM1 maintains the leukemic state through HOX expression. Cancer Cell 2018;34:499–512.
4. Jeanne M, Lallemand-Breitenbach V, Ferhi O, Koken M, Le Bras M, Duffort S, et al. PML/RARA oxidation and arsenic binding initiate the antileukemia response of As2O3. Cancer Cell 2010;18:88–98.
5. Niwa-Kawakita M, Ferhi O, Soilihi H, Le Bras M, Lallemand-Breitenbach V, de The H. PML is a ROS sensor activating p53 upon oxidative stress. J Exp Med 2017;214:3197–206.
6. Ablain J, Rice K, Soilihi H, de Reynies A, Minucci S, de The H. Activation of a promyelocytic leukemia-tumor protein 53 axis underlies acute promyelocytic leukemia cure. Nat Med 2014;20:167–74.
7. Lehmann-Che J, Bally C, de The H. Therapy resistance in APL. New Engl J Med 2014;371:1171–2.
8. de The H, Pandolfi PP, Chen Z. Acute promyelocytic leukemia: a paradigm for oncoprotein-targeted cure. Cancer Cell 2017;32:552–60.
9. Carracedo A, Weiss D, Leliaert AK, Bhasin M, de Boer VC, Laurent G, et al. A metabolic prosurvival role for PML in breast cancer. J Clin Invest 2012;122:3088–100.
10. Ito K, Carracedo A, Weiss D, Arai F, Ala U, Avigan DE, et al. A PML-PPAR-delta pathway for fatty acid oxidation regulates hematopoietic stem cell maintenance. Nat Med 2012;18:1350–8.
11. Gentric G, Kieffer Y, Mieulet V, Goundiam O, Bonneau C, Nemati F, et al. PML-regulated mitochondrial metabolism enhances chemosensitivity in human ovarian cancers. Cell Metab 2019;29:156–73.
12. van Galen P, Mbong N, Kreso A, Schoof EM, Wagenblast E, Ng SWK, et al. Integrated stress response activity marks stem cells in normal hematopoiesis and leukemia. Cell Rep 2018;25:1109–17.
13. Letai A. Functional precision cancer medicine-moving beyond pure genomics. Nat Med 2017;23:1028–35.
14. Farge T, Saland E, de Toni F, Aroua N, Hosseini M, Perry R, et al. Chemotherapy-resistant human acute myeloid leukemia cells are not enriched for leukemic stem cells but require oxidative metabolism. Cancer Discov 2017;7:716–35.
15. Pollyea DA, Stevens BM, Jones CL, Winters A, Pei S, Minhajuddin M, et al. Venetoclax with azacitidine disrupts energy metabolism and targets leukemia stem cells in patients with acute myeloid leukemia. Nat Med 2018;24:1859–66.
16. Sharon D, Cathelin S, Mirali S, Di Trani JM, Yanofsky DJ, Keon KA, et al. Inhibition of mitochondrial translation overcomes venetoclax resistance in AML through activation of the integrated stress response. Sci Transl Med 2019;11:eaax2863.
17. Aroua N, Boet E, Ghisi M, Nicolau-Travers ML, Saland E, Gwilliam R, et al. Extracellular ATP and CD39 activate cAMP-mediated mitochondrial stress response to promote cytarabine resistance in acute myeloid leukemia. Cancer Discov 2020;10:1544–65.
18. Oresta B, Pozzi C, Braga D, Hurle R, Lazzeri M, Colombo P, et al. Mitochondrial metabolic reprogramming controls the induction of immunogenic cell death and efficacy of chemotherapy in bladder cancer. Sci Transl Med 2021;13:eaba6110.
19. Molina JR, Sun Y, Protopopova M, Gera S, Bandi M, Bristow C, et al. An inhibitor of oxidative phosphorylation exploits cancer vulnerability. Nat Med 2018;24:1036–46.
20. Wallace KB, Sardao VA, Oliveira PJ. Mitochondrial determinants of doxorubicin-induced cardiomyopathy. Circ Res 2020;126:926–41.
21. Beziat G, Tavitian S, Bertoli S, Huguet F, Largeaud L, Luquet I, et al. Dactinomycin in acute myeloid leukemia with NPM1 mutations. Eur J Haematol 2020;105:302–7.
22. Falini B, Brunetti L, Martelli MP. Dactinomycin in NPM1-mutated acute myeloid leukemia. N Engl J Med 2015;373:1180–2.
23. Gionfriddo I, Brunetti L, Mezzasoma F, Milano F, Cardinali V, Ranieri R, et al. Dactinomycin induces complete remission associated with nucleolar stress response in relapsed/refractory NPM1-mutated AML. Leukemia 2021.
24. El Hajj H, Dassouki Z, Berthier C, Raffoux E, Ades L, Legrand O, et al. Retinoic acid and arsenic trioxide trigger degradation of mutated NPM1, resulting in apoptosis of AML cells. Blood 2015;125:3447–54.
25. Martelli MP, Gionfriddo I, Mezzasoma F, Milano F, Pierangeli S, Mulas F, et al. Arsenic trioxide and all-trans retinoic acid target NPM1

mutant oncoprotein levels and induce apoptosis in NPM1-mutated AML cells. Blood 2015;125:3455–65.
26. Loberg MA, Bell RK, Goodwin LO, Eudy E, Miles LA, SanMiguel JM, et al. Sequentially inducible mouse models reveal that Npm1 mutation causes malignant transformation of Dnmt3a-mutant clonal hematopoiesis. Leukemia 2019;33:1635–49.
27. Zou Q, Tan S, Yang Z, Zhan Q, Jin H, Xian J, et al. NPM1 mutant mediated PML delocalization and stabilization enhances autophagy and cell survival in leukemic cells. Theranostics 2017;7:2289–304.
28. Huang M, Thomas D, Li MX, Feng W, Chan SM, Majeti R, et al. Role of cysteine 288 in nucleophosmin cytoplasmic mutations: sensitization to toxicity induced by arsenic trioxide and bortezomib. Leukemia 2013;27:1970–80.
29. Weerapana E, Wang C, Simon GM, Richter F, Khare S, Dillon MB, et al. Quantitative reactivity profiling predicts functional cysteines in proteomes. Nature 2010;468:790–5.
30. Sportoletti P, Grisendi S, Majid SM, Cheng K, Clohessy JG, Viale A, et al. Npm1 is a haploinsufficient suppressor of myeloid and lymphoid malignancies in the mouse. Blood 2008;111:3859–62.
31. Kwon J, Bakhoum SF. The cytosolic DNA-sensing cGAS-STING pathway in cancer. Cancer Discov 2020;10:26–39.
32. Riley JS, Tait SW. Mitochondrial DNA in inflammation and immunity. EMBO Rep 2020;21:e49799.
33. Huang Y, Wang S, Zhou J, Liu Y, Du C, Yang K, et al. IRF1-mediated downregulation of PGC1alpha contributes to cardiorenal syndrome type 4. Nat Commun 2020;11:4664.
34. Bursac S, Brdovcak MC, Pfannkuchen M, Orsolic I, Golomb L, Zhu Y, et al. Mutual protection of ribosomal proteins L5 and L11 from degradation is essential for p53 activation upon ribosomal biogenesis stress. Proc Natl Acad Sci U S A 2012;109:20467–72.
35. Choong ML, Yang H, Lee MA, Lane DP. Specific activation of the p53 pathway by low dose actinomycin D: a new route to p53 based cyclotherapy. Cell Cycle 2009;8:2810–8.
36. West AP, Khoury-Hanold W, Staron M, Tal MC, Pineda CM, Lang SM, et al. Mitochondrial DNA stress primes the antiviral innate immune response. Nature 2015;520:553–7.
37. Wiley CD, Velarde MC, Lecot P, Liu S, Sarnoski EA, Freund A, et al. Mitochondrial dysfunction induces senescence with a distinct secretory phenotype. Cell Metab 2016;23:303–14.
38. Mallardo M, Caronno A, Pruneri G, Raviele PR, Viale A, Pelicci PG, et al. NPMc+ and FLT3_ITD mutations cooperate in inducing acute leukaemia in a novel mouse model. Leukemia 2013;27:2248–51.
39. Bajpai R, Sharma A, Achreja A, Edgar CL, Wei C, Siddiqa AA, et al. Electron transport chain activity is a predictor and target for venetoclax sensitivity in multiple myeloma. Nat Commun 2020;11:1228.
40. DiNardo CD, Tiong IS, Quaglieri A, MacRaild S, Loghavi S, Brown FC, et al. Molecular patterns of response and treatment failure after frontline venetoclax combinations in older patients with AML. Blood 2020;135:791–803.
41. DiNardo CD, Jonas BA, Pullarkat V, Thirman MJ, Garcia JS, Wei AH, et al. Azacitidine and venetoclax in previously untreated acute myeloid leukemia. N Engl J Med 2020;383:617–29.
42. Inoue S, Li WY, Tseng A, Beerman I, Elia AJ, Bendall SC, et al. Mutant IDH1 Downregulates ATM and Alters DNA Repair and Sensitivity to DNA Damage Independent of TET2. Cancer Cell 2016;30:337–48.
43. Sahin U, Ferhi O, Jeanne M, Benhenda S, Berthier C, Jollivet F, et al. Oxidative stress-induced assembly of PML nuclear bodies controls sumoylation of partner proteins. J Cell Biol 2014;204:931–45.
44. Missiroli S, Bonora M, Patergnani S, Poletti F, Perrone M, Gafa R, et al. PML at mitochondria-associated membranes is critical for the repression of autophagy and cancer development. Cell Rep 2016;16:2415–27.
45. Mendez-Ferrer S, Bonnet D, Steensma DP, Hasserjian RP, Ghobrial IM, Gribben JG, et al. Bone marrow niches in haematological malignancies. Nat Rev Cancer 2020;20:285–98.
46. Batsivari A, Haltalli MLR, Passaro D, Pospori C, Lo Celso C, Bonnet D. Dynamic responses of the haematopoietic stem cell niche to diverse stresses. Nat Cell Biol 2020;22:7–17.
47. Humeau J, Sauvat A, Cerrato G, Xie W, Loos F, Iannantuoni F, et al. Inhibition of transcription by dactinomycin reveals a new characteristic of immunogenic cell stress. EMBO Mol Med 2020;12:e11622.
48. Tigano M, Vargas DC, Tremblay-Belzile S, Fu Y, Sfeir A. Nuclear sensing of breaks in mitochondrial DNA enhances immune surveillance. Nature 2021;591:477–81.
49. Morganti C, Bonora M, Ito K, Ito K. Electron transport chain complex II sustains high mitochondrial membrane potential in hematopoietic stem and progenitor cells. Stem Cell Res 2019;40:101573.
50. Guo S, Cheng X, Lim JH, Liu Y, Kao HY. Control of antioxidative response by the tumor suppressor protein PML through regulating Nrf2 activity. Mol Biol Cell 2014;25:2485–98.
51. Dagher T, Maslah N, Edmond V, Cassinat B, Vainchenker W, Giraudier S, et al. JAK2V617F myeloproliferative neoplasm eradication by a novel interferon/arsenic therapy involves PML. J Exp Med 2021;218:e20201268.
52. Dos Santos GA, Abreu ELRS, Pestana CR, Lima AS, Scheucher PS, Thome CH, et al. (+)alpha-Tocopheryl succinate inhibits the mitochondrial respiratory chain complex I and is as effective as arsenic trioxide or ATRA against acute promyelocytic leukemia in vivo. Leukemia 2012;26:451–60.
53. Zucenka A, Pileckyte R, Trociukas I, Peceliunas V, Vaitekenaite V, Maneikis K, et al. Outcomes of relapsed or refractory acute myeloid leukemia patients failing venetoclax-based salvage therapies. Eur J Haematol 2021;106:105–13.